VIII International Conference on Fracture Mechanics of Concrete and Concrete Structures
FraMCoS-8
J.G.M. Van Mier, G. Ruiz, C. Andrade, R.C. Yu and X.X. Zhang (Eds)

NUMERICAL MODELLING OF THE TENSILE SPLITTING TEST AND ITS COUPLING WITH GAS PERMEABILITY

N. BENKEMOUN*, X. JOURDAIN†, M. CHOINSKA* AND A. KHELIDJ*

*LUNAM Université, GeM, UMR CNRS 6183
IUT de Saint Nazaire, Université de Nantes, France
e-mail: nathan.benkemoun@univ-nantes.fr

†LMT-Cachan (ENS-Cachan/CNRS/UPMC/PRES UniverSud Paris)
61 avenue du Président Wilson, 94235 Cachan Cedex, France
e-mail: jourdain@lmt.ens-cachan.fr

Key words: Cracking, Permeability, Strong Discontinuity approach, Poiseuille law, Tensile splitting test

Abstract. The aim of this paper is to investigate interactions between cracking and permeability in the tensile splitting test. Two models are briefly introduced: the first one is dedicated to the concrete modelling at the meso-scale by means of the Enhanced Finite Element Method; the second one is used for the coupling between cracking and permeability. Finally, numerical computations are performed and some comparisons with experimental data are presented.

1 INTRODUCTION

In litterature, some experimental results attempting to understand the mutual interaction and relationship between concrete cracks and the permeability of concrete by means of controlled splitting tests can be found. Controlled splitting tests are used to create cracks produced by tensile stress in cylindrical concrete samples. These tests have stressed a correlation between water permeability ([1]) or chloride diffusion ([2]) and the crack opening width, but only if the crack opening displacement (COD) is greater than 50 μm (under this value there is no significative increase of the values in the permeability matrix). Gas permeability tests have also been experimented (see [3]). Results show that the gas permeability markedly increases for a COD of about 25 μm. Therefore it appears that gas permeability is more sensitive than water permeability to cracks induced by loading in concrete. However few papers exist regarding the bibliography dealing with the numerical modelling of these Brazilian splitting tests and the coupling with permeability (either water or gas). One can cite, even if it's for a compressive loading and so it is out of the scope of this study, the one of [4], where with the help of a lattice (mechanical and hydraulic) analyses, the authors find a numerical correlation between the value of the crack opening and the gas permeability, and compare their results to the work of [5]. Their interest is limited to the phase where only micro-cracks have been formed (diffuse distribution of cracks), and thus a connected network resulting in a macro-crack is not yet present. The link between permeability around the peak regime or in the softening regime has not been studied in the context of their paper. Concerning the numerical modelling of the Brazilian splitting test, one can note a technical paper of [6] where by using a non local elastic-damage model in the context of the Finite Element method, the authors

are able to reproduce with accuracy the complex failure mechanism of this test. This model has then been enhanced by the key idea developed in [7] permitting to extract a crack opening from a continuum damage Finite Element computation and thus to develop a model coupling crack opening and permeability in the context of the continuum damage mechanics (see [8], [9]). Contrary to [4], the authors are able to reproduce the whole regime of growth of the permeability from diffuse to localised damage. Thus, the proposed work is a contribution to these papers: modelling the tensile splitting test and its coupling with gas permeability in the context of the Strong Discontinuity approach (see [10]).

The outline of this paper is as follows: In Section 2, we give a brief description of the meso-scale model of concrete developed in [11] which is used to model the tensile splitting test. In Section 3, we provide a short review of the hydro-mechanical coupling model developed in [12], making the link between the process of cracking and permeability. In Section 4, we turn to the example of the tensile splitting test. First, some mechanical computations are exposed and then hydro-mechanical coupling results are presented. Finally, some comparisons with experimental data from [9] are provided.

2 Meso-scale model for cracking modelling in concrete-like materials

In this section, a brief description of a two-phase material (such as concrete) model at the meso-scale is given. For readers interested in more details, a full description of the model, its numerical implementation and some examples showing the model capabilities and its range of applications can be found in [11] and [13].

2.1 Mechanical meso-scale model features

Being able to take into account the size, influence of the shape, and the mechanical properties of aggregates on the mechanical behaviour of concrete-like materials appear to be of interest, that's why the model proposed in [11] is based upon a two-phase (aggregates melt into a mortar matrix) quasi-brittle Finite Element model whose meso-scale is chosen to be the scale of computation. Thanks to this model, the behavior of concrete-like materials under mechanical loading paths can be represented. From a technical point of view, the meso-scale model for computations is based upon a 3D lattice Finite Element model ([14] and [15]), whose truss elements kinematics have been enhanced by two discontinuities.

The first discontinuity is known in litterature by the term of weak discontinuity (continuous displacement field and discontinuous strain field, see [16]). This discontinuity is introduced in relation with the retained meshing process, namely non-conforming meshes (see [17]) involving some truss elements that are cut into two parts, each having different elastic properties. The main advantage is to have a meshing process independent from the microstructure (positions and shapes of the aggregates). In the present work, this approach is applied to samples used for the tensile splitting test. Fig. 1 represents one of them: a cylinder with a diameter of 110 mm and a thickness of 3 mm. The Finite Element discretization gives three sets of truss elements: (1) those entirely inside the matrix (in blue) with no weak discontinuity activated; (2) those entirely in the aggregates (in green color) with no weak discontinuity activated and (3) those split by a physical interface (in red) for which the weak discontinuity is activated.

The second discontinuity is based upon a strong discontinuity (discontinuous displacement field and unbounded strain field, see [10]). One can note that this discontinuity is introduced with the aim of representing microcracks that can appear in any of the two phases (aggregates or mortar matrix) and of capturing the debonding at the interfaces between aggregates and the mortar matrix. It is important to stress the fact that strong discontinuities using gives the capability to model softening behavior without any mesh dependency, (see [18]).
In order to introduce the softening behaviour, a softening law is introduced in terms of the in-

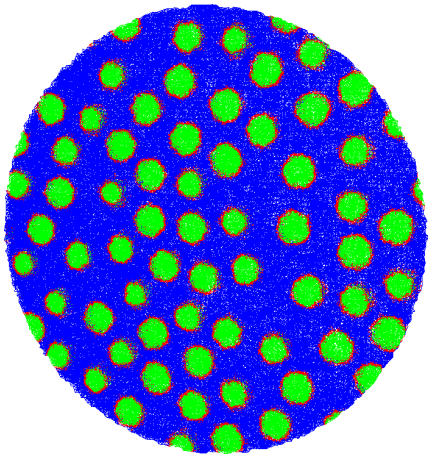

Figure 1: Cylindrical sample for the brazilian test

ternal variable q by considering the exponential form

$$q = \sigma_u(1 - exp(-\frac{[|u|]\sigma_u}{G_f})) \qquad (1)$$

with G_f, $[|u|]$ and σ_u respectively the fracture energy, the crack opening and the tensile strength before softening. Finally, in order to introduce this strong discontinuity, a yield function Φ, triggered only in traction, is adopted such as

$$\Phi = t_\Gamma - (\sigma_u - q) \qquad (2)$$

with t_Γ the traction vector at the discontinuity.

2.2 Solving process

The introduction of these discontinuities in a Finite Element problem is done by means of the Hu-Washizu three fields variational formulation (see [19]) and their discretization is realised by the mean of the Enhanced Finite Element Method (E-FEM). In a nutshell, the principal of this method is to enhance the deformation field by two functions $G^{1/2}$ and G_2 corresponding respectively to weak and to strong discontinuities. On each element cut into two parts and/or which has reached σ_u, interpolation parameters are computed (one for each function) with a local algorithm. Note that one of the interpolation parameters is nothing but the crack opening $[|u|]$. When the local convergence is reached and the values of these two interpolation parameters obtained, a static condensation is performed; then, a classical Finite Element problem is solved except that the stiffness matrix takes into account coefficients coming from the static condensation. The whole computational procedure is explained in detail in [11].

3 Meso-scale model for hydo-mechanical coupling problem in a cracked media

In this section, a short review of the hydro-mechanical coupling model used to make the link between cracking and permeability at the meso-scale is provided. For readers interested in more details, a full description of the model, its numerical implementation and some examples can be found in [12] and [20].

3.1 Hydro-mechanical coupling model features

The key point of the hydro-mechanical coupling is based upon the fact that the crack opening $[|u|]$ is computed when solving the mechanical problem at the meso-scale. This data leads to a straightforward way to compute mass flows within meso-scale cracks according to the Poiseuille law written in the case of two infinite parallel planes with a distance equals to $[|u|]$. Moreover, it appears that this mass flow problem will inherit from information coming from the mechanical analysis namely different crack openings and orientations and thus the hydro-mechanical coupling will naturally take into account fracture tortuosity and induced anisotropy

which is usually, except for low stress levels, a difficult task (see [21]).
Considering an incompressible fluid passing through a cracked media, one can compute the permeability tensor as

$$\underline{\underline{K}}^m = k_{intr}\underline{\underline{1}} + \frac{[|u|]^3}{12L}(\underline{\underline{1}} - \underline{n} \otimes \underline{n}) \qquad (3)$$

where $\underline{n}$ is the truss unit normal vector, k_{intr} is the intrinsic permeability of the material (e.g. 10^{-17} m^2 for ordinary concrete) and L is the length of the crack. One can observe that a double porosity is taken into account : one isotropic coming from the intrinsic porosity (k_{intr}) of the considered uncracked material and one anisotropic coming from the mechanical computation in terms of meso-scale cracks opening ($[|u|]$).
The corresponding mass flow density vector $\underline{q}$ is thus:

$$\underline{q} = -\rho\frac{\underline{\underline{K}}^m}{\mu} \cdot \underline{grad}(p) \qquad (4)$$

When considering a compressible gas, the density ρ of the fluid cannot be assumed to remain constant and $\underline{q}$ must be rewritten as

$$\underline{q} = -\frac{\underline{\underline{K}}^m}{2\mu}\frac{M}{RT} \cdot \underline{grad}(p^2) \qquad (5)$$

where M is the molar mass (kg.mol^{-1}), R is the universal gas constant (8.314 J.K^{-1}.mol^{-1}), μ is the viscosity of the fluid (Pa.s) and T is the absolute temperature (K).

3.2 Solving process

The solving process is based upon a Finite Element formulation of the flow problem at the meso-scale. First, the weak form of the mass balance equation is obtained and then the Finite Element spatial discretization of the pressure field (for an incompressible problem) or the pressure-squared field (for a compressible problem, [22], [23]), the gradient operator and the permeability matrix is executed. Finally by applying the Finite Element assembly procedure, the resolution of the problem in terms of pressure field or pressure-squared field is performed. The whole computational procedure is explained in detail in [12].

In the next Section, we turn to the example of the tensile splitting test in order to illustrate the capabilities of the mechanical model and the hydro-mechanical coupling.

4 Numerical example: Tensile splitting test

In the first section, we demonstrate the mechanical results obtained with the model. In the second section, results of the hydro-mechanical coupling are presented. These results are then discussed.

4.1 Mechanical results

Mechanical computations are performed on cylindrical samples (such as Fig. 1) with dimensions and material properties detailed in Tab. 4.1. Three samples are tested with different diameter inclusions sizes $\Phi_{inclusions}$ (2, 4 and 8 mm) keeping the volume of inclusions constant. In order to impose boundaries conditions, two planes are cut on the top and on the bottom of the cylinder. On the top the loading is imposed by prescribing a vertical displacement and on the bottom the sample is blocked in the x, y and z directions. The vertical load is thus computed as the corresponding reaction.

Fig. 2 represents the stress versus the maximum crack opening displacement (COD$_{max}$) for each loading paths and for $\Phi_{inclusions}$ equal to 8, 4 and 2 mm. One can observe that the peak is reached for an average stress value of 8.4 MPa and an average maximum crack opening displacement value of 10.5 μm. We have tried to highlight a trend between the size of the aggregates and the value of the Young modulus, the value of the stress at the peak. The result is pictured on Fig. 3. Regarding this picture, it is not clear, there is a trend but it seems that values of the Young modulus and the stress at the peak are going up with the size of the aggregates. Moreover, Fig. 2 shows that smaller the size of inclusions, the more brittle the response.

Fig. 4 illustrates the evolution of the crack by the mechanical loading after the peak for $\Phi_{inclusions}$ equals to 8 mm. The path of the

Table 1: Dimensions and material properties

Cylinder dimensions (mm)	ϕ = 110 & e = 3		
Samples name	1	2	3
$\Phi_{inclusions}$ (mm)	8	4	2

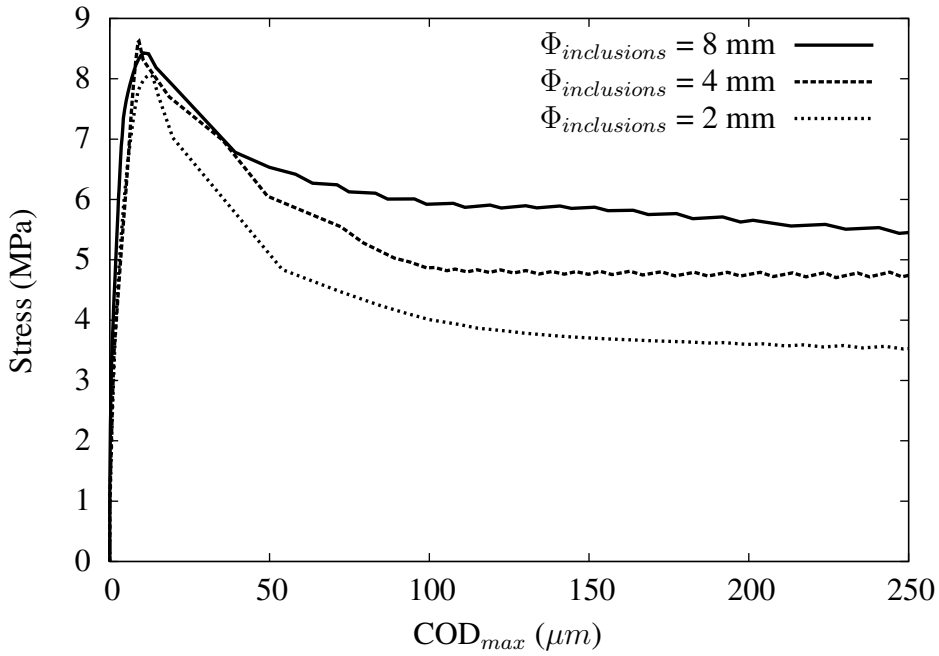

Figure 2: Stress versus COD$_{max}$ [0 to 250 μm]

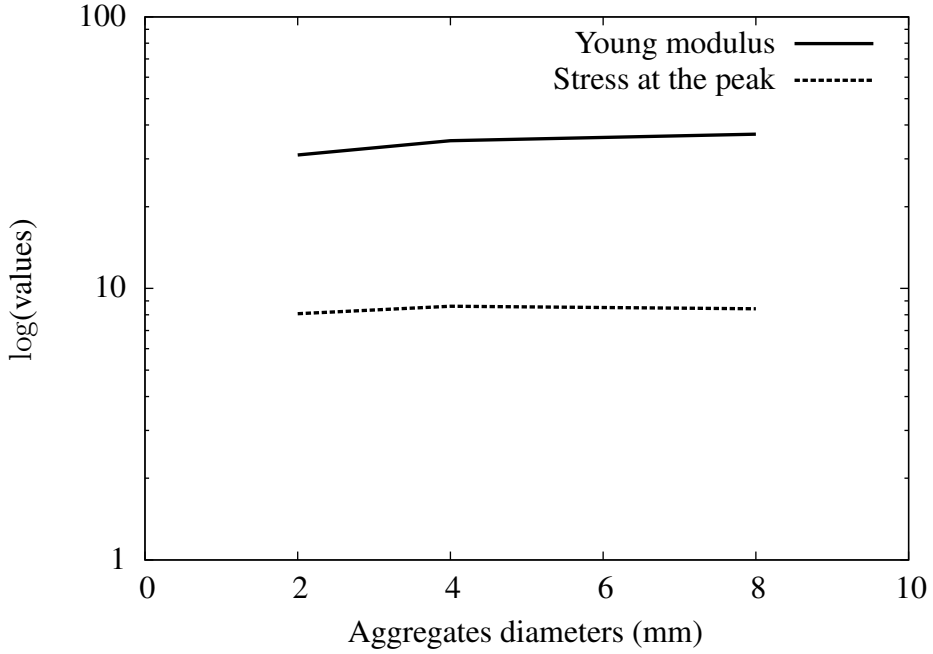

Figure 3: Values of the log(Young modulus, COD$_{max\,at\,the\,peak}$, Stress at the peak) versus the size of the aggregates

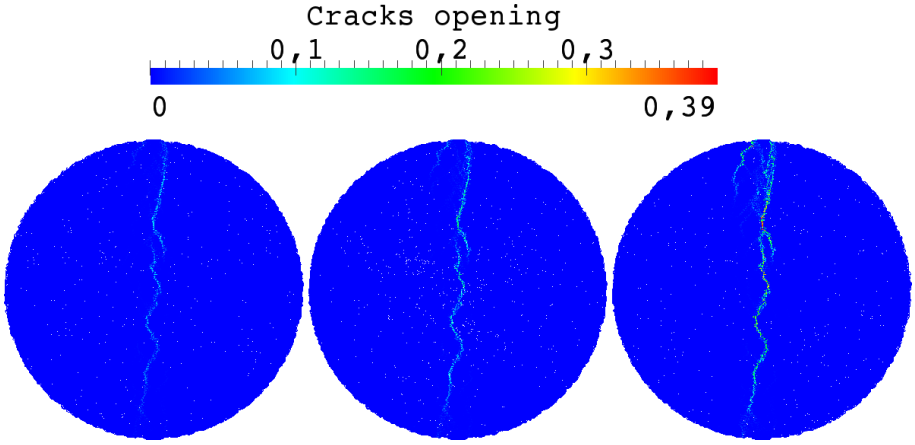

Figure 4: Evolution of the crack by the mechanical loading ($\Phi_{inclusions}$ = 8 mm): COD_{max} (μm) = 100, 160 and 390

crack is tortuous because it follows the aggregates which remain elastic. Note: values in the colorbar are in mm.

In the next section, we turn to hydro-mechanical results obtained from these cracked samples.

4.2 Hydro-mechanical results and discussion

In order to solve the mass transfer problem, a pressure called P_{in} is imposed in the z-direction on the face z = 0 mm such as P_{in} = 2×10^5 Pa and a pressure called P_{out} is imposed in the z-direction on the face z = 3 mm such as P_{out} = 1×10^5 Pa. The gas considered is air, thus M is equal to 0.02895 kg.mol^{-1} and μ to 1.82×10^{-5} Pa.s. The intrinsic permeability of the inclusions is chosen equal to 10^{-25} m^2 and the one of the mortar matrix to 10^{-16} m^2.

Fig. 5 shows results of the permeability computation. It pictures the log of the Permeability/Initial Permeability versus the COD_{max}. One can observe three regimes (with the help of Fig. 2 too) regardless of the size of the inclusions; the first one going almost to the $\text{COD}_{max\,at\,the\,peak}$. It shows a slow increase of the permeability because of the increase of the density of diffuse (micro) cracks. Because of the coalescence of the micro-cracks leading to a macro-crack, a second regime of permeability can be observed. It exhibits around the peak a fast increase of the permeability. These two regimes are quite illustrated on Fig. 6 which is a zoom of Fig. 5 for a COD ranging from 0 to 50 μm. It depicts the log of the Permeability/Initial Permeability versus the COD_{max}. One can observe, around a value of 10 μm, a fast increase of the permeability. Finally, and for a COD_{max} larger than several times the $\text{COD}_{max\,at\,the\,peak}$, a third regime is observed which is characterized by a slower growth of the permeability (see Fig. 5 again). Last but not least, it is important to stress the fact that the presence of these three regimes is in good agreement with what one can observed experimentally (see [24] for instance).

One can note that all these computations have been performed with three sizes of inclusions (2, 4 and 8 mm); the aim being to investigate the influence of the size of the inclusions in relation with the permeability as done in the work of [25]. Regarding Fig. 5 and Fig. 6 it is not easy to find a trend between the size of the aggregates and the evolution of permeability. Nevertheless Fig. 5 tends to show that whatever the size of inclusions is, the second regime starts at the same time (around 10 μm here).

Finally regarding Fig. 7, one can compare numerical results with the experimental data from [9]. The experimental results have been obtained considering 4 Brazilian test samples (A, B, C and D) with thickness from 3 cm to 5 cm and a size of inclusions of 4 mm of diameter. Even if the numerical results are in good agreement with the experimental values, this comparison must be done with precaution. Indeed, the thickness of the numerical sample has been cho-

sen equal to 3 mm for computational time reason and so is far away from the thickness used in experiment. The numerical simulation is thus much closer to a 2D simulation than a 3D simulation. Moreover, in the numerical approach no coefficient is introduced in order to take into account the rugosity of the crack: this could explain too the higher rate of growth of permeability for the numerical approach ragarding the experimental one. For further computations it would be of interest to introduce this coefficient following for the work of [3].

5 ACKNOWLEDGEMENTS

The financial support of the Agence Nationale de la Recherche through the non thematic program (contract NT09_541416, acronym ECOBA), the Fonds Unique Interministériel through the collaborative research and development program MAREVA (contract AAP7 0192-03) and the FEDER/CPER research grants is gratefully acknowledged.

6 CONCLUSION

The aim of this paper was to investigate interactions between cracking and permeability in the context of the tensile splitting test. In the first part of this work, the key points of the mechanical model were presented: two discontinuities have been introduced in order to model cracking in heterogeneous materials. Then, in the second part the hydro-mechanical coupling was briefly introduced, it relies on a double porosity approach permitting to build up a permeability matrix taking into account cracks opening and their orientations. Finally, some numerical computations dealing with the hydro-mechanical coupling in the context of the Brazilian splitting test have been shown. Several results have been obtained. First, the presence of three regimes of permeability have been highlighted as observed in experimental approaches. The first regime, going almost to the peak, is governed by the intrinsic porosity of the material and shows a slow increase of the permeability, then around the peak, when there is coalescence of micro-cracks that gives a macro-crack, one can observed a second regime with a fast growth of the permeability (between two and three decades) and finally a third regime is observed for a displacement larger than the one at the peak with a slower rate of growth of permeability. Then, concerning the influence of the size of the inclusions in relation with the permeability, one can note that whatever the size is, the second regime of permeability starts practically at the same time (around 10 μm). Even if these results are encouraging for further works, several things have to be improved. Concerning the mechanical simulation of the tensile splitting test, boundaries conditions should be imposed more neatly namely by respecting what is done in [26]. This should be done in modelling the bearing strip in steel and so the contact between concrete and steel. Then, it should be important to work with a sample thickness in the range of experimental approaches namely in between 3 and 5 cm. In this work, because of computational time, the thickness had to be chosen equal to 3 mm which is far away from real samples. Changing the thickness could be a first lead to improve the comparison with experimental results (see Fig. 7). Regarding the hydro-mechanical coupling, no rugosity coefficient has been introduced in order to model the rugosity of the crack. Therefore the influence of this rugosity is not taken into account in the computation; this could be a second lead to improve the comparison with experimental results. Several authors have identified this coefficient using experimental data (see [3]).

To conclude, future works will have to improve the predictions of permeability with experimental data on split cylinders even if initial comparisons provide qualitative and quantitative results that are quite enough consistent.

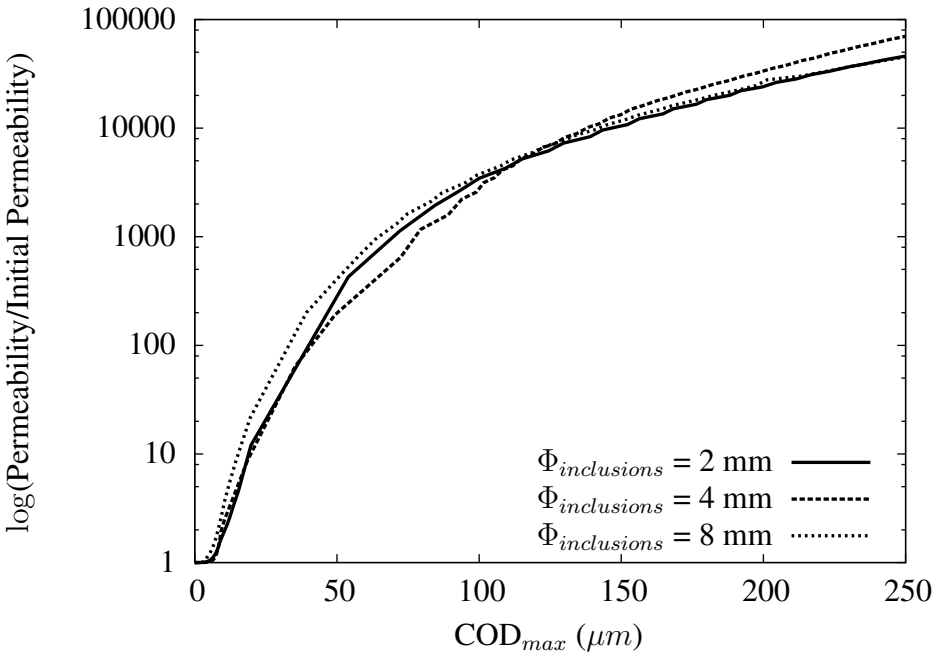

Figure 5: log(Permeability/Initial Permeability) versus COD$_{max}$ ([0 to 250 μm])

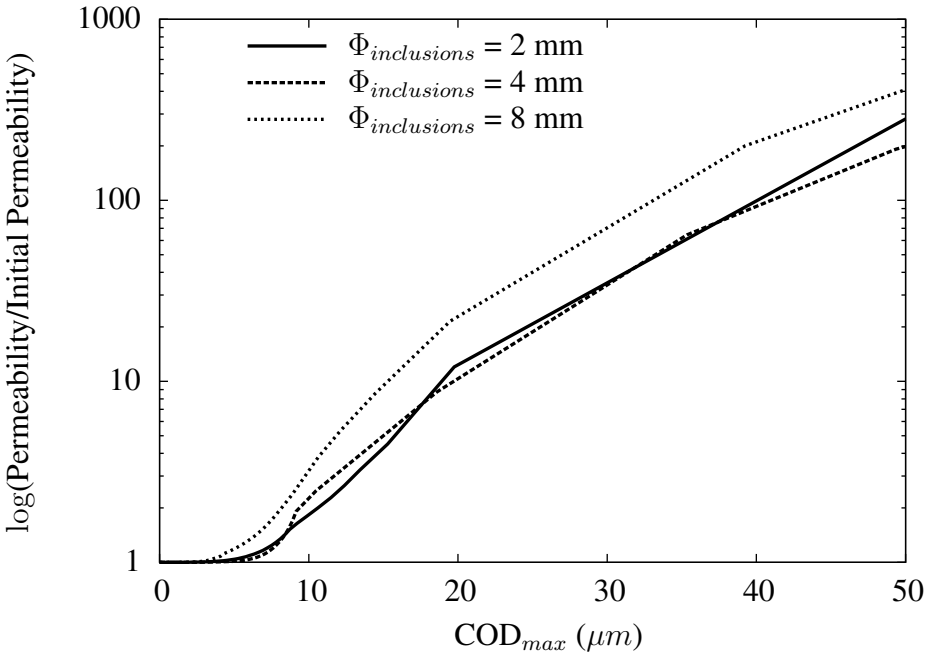

Figure 6: log(Permeability/Initial Permeability) versus COD$_{max}$ ([0 to 50 μm])

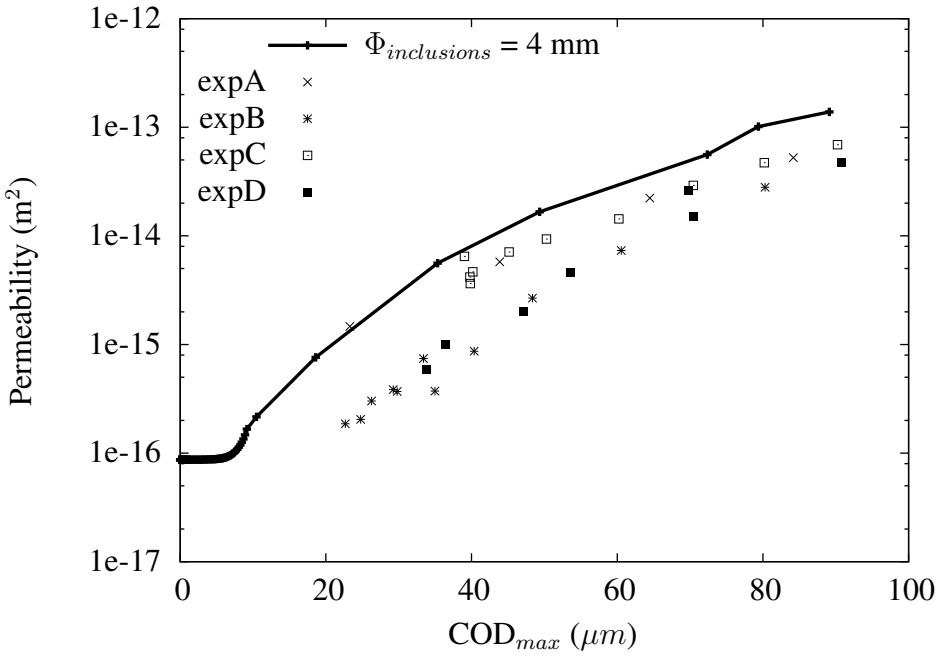

Figure 7: Permeability versus COD$_{max}$ / experimental data ([9])

REFERENCES

[1] K. Wang, D. Jansen, and S. Shah, "Permeability study of cracked concrete," *Cement and Concrete Research*, vol. 27, pp. 381–393, 1997.

[2] A. Djerbi, S. Bonnet, and V. Baroghelbouny, "Influence of traversing crack on chloride diffusion into concrete," *Cement and Concrete Research*, vol. 38, pp. 877–883, 2008.

[3] V. Picandet, A. Khelidj, and H. Bellegou, "Crack effect on gas and water permeability of concrete," *Cement and Concrete Research*, vol. 39, pp. 537–547, 2009.

[4] G. Chatzigeorgiou, V. Picandet, A. Khelidj, and G. Pijaudier-Cabot, "Coupling between progressive damage and permeability of concrete: analysis with a discrete model," *International Journal for Numerical and Analytical Methods in Geomechanics*, vol. 29, pp. 1005–1018, 2005.

[5] V. Picandet, A. Khelidj, and G. Bastian, "Effect of axial compressive damage on gas permeability of ordinary and high-performance concrete," *Cement and Concrete Research*, vol. 31, pp. 1525–1532, 2001.

[6] A. Rodriguez-Ferran and A. Huerta, *Failure and post-failure modelling of the brazilian test*. Trends in Computational Structural Mechanics, W.A. Wall, K.-U. Bletzinger and K. Schweizerhof (Eds.): CIMNE, Barcelona, Spain, 2001.

[7] F. Dufour, G. Pijaudier-Cabot, M. Choinska, and A. Huerta, "Extraction of a crack opening from a continuous approach using regularized damage model," *Computers and Concrete*, vol. 4, pp. 375–388, 2008.

[8] G. Pijaudier-Cabot, F. Dufour, and M. Choinska, "Damage and permeability in quasi-brittle materials : from diffuse to localised properties.,"

[9] M. Choinska, F. Dufour, G. Pijaudier-Cabot, A. Huerta, and A. Khelidj, "How to extract a crack opening from a continuous damage finite element computa-

tion ? application for the estimation of permeability," GeoProc2008: Proceedings of the 3rd International Symposium GeoProc'2008 (ISTE), 2008.

[10] J. C. Simo, J. Oliver, and F. Armero, "An analysis of strong discontinuities induced by strain-softening in rate independent inelastic solids," *Computational Mechanics*, vol. 12, pp. 277–296, 1993.

[11] N. Benkemoun, M. Hautefeuille, J.-B. Colliat, and A. Ibrahimbegovic, "Modeling heterogenous materials failure: 3D meso-scale models with embedded discontinuities," *International Journal for Numerical Methods in Engineering*, vol. 82, pp. 1671–1688, 2010.

[12] X. Jourdain, A. Valade, J.-B. Colliat, C. De Sa, F. Benboudjema, and F. Gatuingt, "Upscaling permeability for fractured concrete: meso-macro numerical approach coupled to strong discontinuities," *International Journal for Numerical and Analytical Methods in Geomechanics*, vol. 0, p. submitted, 2011.

[13] N. Benkemoun, J.-B. Colliat, and A. Ibrahimbegovic, "Anisotropic constitutive model of plasticity capable of accounting for details of meso-structure of two-phase composite material," *Computers and Structures*, vol. 90–91, pp. 153–162, 2012.

[14] E. Schlangen and J. G. M. van Mier, "Simple lattice model for numerical simulation of fracture of concrete materials and structures," *Materials and Structures*, vol. 25, pp. 534–542, 1992.

[15] E. Schlangen and E. J. Garboczi, "Fracture simulations of concrete using lattice models: computational aspects," *Engineering Fracture Mechanics*, vol. 57, pp. 319–332, 1997.

[16] T. Belytschko, J. Fish, and B. Engelmann, "A finite element with embedded localization zones," *Computer Methods in Applied Mechanics and Enginnering*, vol. 70, pp. 59–89, 1988.

[17] N. Moës, M. Cloirec, P. Cartraud, and J.-F. Remacle, "A compuational approach to handle complex microstructure geometries," *Computer Methods in Applied Mechanics and Engineering*, vol. 192, pp. 3163–3177, 2003.

[18] G. Wells and L. Sluys, "Three-dimensional embedded discontinuity model for brittle fracture," *International Journal of Solids and Structures*, vol. 38, pp. 897–913, 2001.

[19] K. Washizu, *Variational methods in elasticity and plasticity*. New York: Pergamon Press, 3 ed., 1982.

[20] X. Jourdain, A. Valade, J.-B. Colliat, C. De Sa, F. Benboudjema, and F. Gatuingt, "Calcul de la perméabilité en milieu fissuré : approche meso-macro," Transfert 2012, 2012.

[21] G. Pijaudier-Cabot, F. Dufour, and M. Choinska, "Permeability due to the increase of damage in concrete : From diffuse to localized damage distributions," *Journal of Engineering Mechanics*, vol. 135, pp. 1022–1028, 2009.

[22] J. Bear, *Dynamics of Fluids in Porous Media*. Dover Publications, 1972.

[23] F. Brezzi and M. Fortin, *Mixed and hybrid finite element methods*. Springer-Verlag, 1991.

[24] M. Choinska, A. Khelidj, G. Chatzigeorgiou, and G. Pijaudier-Cabot, "Effects and interactions of temperature and stress-level related damage on permeability of concrete," *Cement and Concrete Research*, vol. 37, pp. 79–88, 2007.

[25] A. Fabien, M. Choinska, S. Bonnet, A. Pertué, and A. Khelidj, "Etude expérimentale des effets de la taille de granulat sur le comportement mécanique et la perméabilit au gaz du béton," Actes du colloque national sur les propriétés de transfert des géomatériaux (TRANSFERT 2012), (Ecole Centrale de Lille, Editeurs : Skoczylas F., Davy C., Agostini F., Burlion N., ISBN 978-2-915913-28-6, pp. 313-322.), 2012.

[26] S. Timoshenko and J. Goodier, *Theory of elasticity*. New York: McGraw-Hill, 1970.